batteries

MDPI

Article

Comprehensive Study of the Gas Volume and Composition Generated by 5 Ah Nickel Manganese Cobalt Oxide (NMC) Li-Ion Pouch Cells Through Different Failure Mechanisms at Varying States of Charge

Gemma E. Howard *, Katie C. Abbott, Jonathan E. H. Buston, Jason Gill, Steven L. Goddard and Daniel Howard

HSE Science and Research Centre, Harpur Hill, Buxton SK17 9JN, UK
* Correspondence: gemma.howard@hse.gov.uk

Abstract: Lithium-ion batteries risk failing when subjected to different abuse tests, resulting in gas and flames. In this study, 5 Ah nickel manganese cobalt oxide (NMC) pouch cells were subjected to external heating; overcharge at rates of 2.5, 5 and 10 A; and nail penetration. Tests were conducted in air and N_2 atmospheres. Additional external heat tests were performed on cells at 5, 25, 50, and 75% SoC and on two, three, and four cell blocks. Gas volumes were calculated, and the gas composition was given for H_2, CO, CO_2, C_2H_4, C_2H_6, CH_4, C_3H_6, and C_3H_8. For tests under an air atmosphere at 100% SoC, the volume of gas varied between abuse methods: 3.9 L (external heat), 6.4 L (overcharge), and 8.9 L (nail penetration). The gas composition was found to predominantly contain H_2, CO_2, and CO for all abuse methods; however, higher concentrations of H_2 and CO were present in tests performed under N_2. External heat tests at different SoCs showed that the gas volume decreased with SoC. Overall, the type of abuse method can have a large effect on the gas volume and composition produced by cell failure.

Keywords: Li-ion; pouch cell; nickel manganese cobalt oxide; external heat; overcharge; nail penetration; gas volume; gas composition

Academic Editor: Xianglin Li

Received: 8 April 2025
Revised: 29 April 2025
Accepted: 12 May 2025
Published: 17 May 2025

Citation: Howard, G.E.; Abbott, K.C.; Buston, J.E.H.; Gill, J.; Goddard, S.L.; Howard, D. Comprehensive Study of the Gas Volume and Composition Generated by 5 Ah Nickel Manganese Cobalt Oxide (NMC) Li-Ion Pouch Cells Through Different Failure Mechanisms at Varying States of Charge. *Batteries* **2025**, *11*, 197. https://doi.org/10.3390/batteries11050197

1. Introduction

Lithium-ion batteries (LIBs) are a ubiquitous choice for consumer electronics, electric vehicles (EVs), and battery energy storage systems (BESSs). Within the UK, one driver towards this increase in LIB use is the UK government's Net Zero Initiative, with the aim to cut greenhouse emissions from energy generation and transportation by 2050 [1]. For applications including EVs and BESSs, the use of pouch format cells over cylindrical or prismatic cells is increasing in popularity due to their lightweight compact design and increasing availability in high capacity [2]. Multiple cells can be used to form modules, which can then be joined together to form battery packs.

The widespread use of Li-ion pouch cells means that it is important to understand the hazards of failing cells, including the failure mechanism, gas volume production, and gas composition. The failure of cells can be initiated by varying abuse methods, including external heating (exposure to high temperature for prolonged periods of time), overcharging (failure to stop the current supply once at 100% state of charge (SoC)), and nail penetration (damage to the cell by mechanical failure). Studies have shown that when failure is initiated via the methods outlined, cells are at risk of entering a thermal runaway

(TR) state. TR is the main stage of cell failure when internal heat produced by the cell exceeds the amount of heat able to dissipate to the surrounding environment, preventing cell cooling [3]. As a consequence of heating, the electrolyte begins to decompose, resulting in the formation of gases inside the cell [4]. The build-up of gases causes the casing of a pouch cell to swell. When pressure can no longer be contained within the cell, it bursts, resulting in cell failure. Cell failure can be characterised by the production of flames, sparks, gas, or a combination of all of these [5].

It is of particular interest to understand the volume and composition of gas generated during failure and the factors which can affect these, such as the failure method, state of charge (SoC), and O_2 availability. Cell chemistry is also known to affect the gas composition. However, only cells with nickel manganese oxide (NMC) chemistry were of interest throughout this study [6].

1.1. Gas Volumes

A common way of determining the volume of gas generated during cell failure involves failing the cell in a sealed vessel, allowing the pressure increase observed during cell failure to be recorded. Pressure data can then be used to calculate gas volumes using the ideal gas equation, which has been quantified for a range of NMC cells failed via external heat under both air and inert atmospheres. The lowest volume of gas was reported by Howard from a 5 Ah pouch cell at standard temperature and pressure (STP), which produced 0.86 L/Ah (4.5 L) under an air atmosphere, which was lower compared to the same cell tested under a N_2 atmosphere, 1.3 L/Ah (6.5 L) [7]. This difference in results between atmospheres is likely due to the amount of combustion that can occur due to O_2 availability. The effect that O_2 availability has on gas volume was demonstrated by Dubaniewicz, who used increasing gas canister sizes to fail cells (3.2 Ah 18650). The volume of gas increased with the canister's size; therefore, O_2 availability increased, producing gas volumes ranging from 2.1 to 2.6 L/Ah [8]. The cell format and capacity also had a slight impact of the gas volume, as reported by Koch, who found that the volume of gas generated ranged between 80 and 160 L depending on the cell's format and capacity, with an overall average of 1.96 L/Ah for both pouch cells and hard case (cylindrical and prismatic) cells [9]. Wei performed testing on single 256 Ah prismatic cells with different Ni contents in a N_2 atmosphere only. These cells were found to produce 1.68–2.56 L/Ah [10]. This was similar to that of a ten-cell block (2.5 Ah Samsung 18650-25R), which produced approximately 2.8 L/Ah [11]. In contrast, the failure of a five-cell 14 Ah pouch cell block by Sturk under N_2 produced a significantly larger gas volume, 21 L/Ah [12].

A comparison of the effect different abuse mechanisms have on gas volume production was reported by Essl, who subjected 60 Ah prismatic and pouch cells to external heat, nail penetration, and overcharge tests under a N_2 atmosphere [13]. The abuse method was found to impact gas volume generation, with overcharge tests producing on average 2.65–2.79 L/Ah more than nail penetration, which produced 1.56 L/Ah, and external heat, which produced 1.77 L/Ah. Willstrand's testing of 157 Ah prismatic cells under an inert atmosphere provided evidence that the volume of gas generated increased with SoC when using external heating, nail penetration, and overcharging as failure mechanisms [14].

1.2. Gas Composition

1.2.1. External Heat

The most common constituents of the gas released during failure are shown to be H_2, CO, CO_2, and small hydrocarbons. Howard found that the concentrations of these compounds vary depending on the atmosphere the cell failed under, with CO_2 increasing in air atmospheres due to complete combustion [7]. Alternatively, the concentration of H_2 and CO was higher under an inert atmosphere due to no O_2 availability for combustion. Zou identified the following compounds in the failure gas of a 78 Ah prismatic cell that failed under an air atmosphere: CO (17.2%), H_2 (13.1%), CO_2 (12.1%), O_2 (7.2%), C_2H_4 (4.4%), C_2H_6, and C_3H_8. Other negligible trace gases were also identified, including C_4H_6, n-C_4H_8, n-C_4H_{10}, *trans*-C_4H_8, C_3H_6, C_2H_2, 1,3-C_4H_6, C_3H_4, *cis*-C_4H_8, and *i*-C_4H_8 [15]. Similar gas compositions (CO_2, CO, H_2, C_2H_4, CH_4, C_2H_6, and C_3H_6) accounted for 99% of the gas volume in tests by Koch [9]. The presence of C_2H_2 was also observed in addition to the gases previously mentioned in a study by Yuan [4]. The quantification of gases produced during the failure of ten 2.5 Ah 18650 cells at 100% SoC under a N_2 atmosphere was performed by Yan [11]. The average concentrations were reported: H_2 (35.4%), CO (32.7%), CO_2 (14.9%), CH_4 (6.9%), C_2H_4 (6.8%), H_2O (1.9%), C_3H_8 (1.0%), and C_2H_6 (0.5%).

1.2.2. Overcharge and Nail Penetration

Fewer gas analysis data are currently available for cells that failed overcharge and nail penetration tests. The presence of CO_2 and CO was detected from the failure of 32 Ah NMC-333 pouch cells at 170, 180, and 190% SoC, with the CO_2 concentration increasing and CO concentration decreasing with SoC [16]. The quantification of CO_2 was attempted by Cai using CO_2 sensors, which reached a maximum concentration of 30,000 ppm, approximately 1200 s after cell failure and at a 213% SoC [17]. Gas sensors were also used to detect the presence of CH_4, C_3H_8 and CO from overcharged 58 and 65 Ah pouch cells [18]. Two nail penetration studies with gas analysis have been performed. An overcharged 40 Ah NMC pouch cell (4.3 V) produced gas containing 155 species, including CO (17,062 ppm), H_2, and CO_2 (not quantified), as well as EMC and ethyl carbonate (EC) [19]. Any other gases identified were trace amounts and therefore negligible. Hoelle failed 25 types of prismatic format (8–145 Ah) cells under an argon atmosphere [20]. Each test was repeated twice and detected H_2 (32 vol%), CO (31 vol%), and CO_2 (28 vol%), with traces of C_2H_4 and C_2H_2.

1.2.3. Multiple Abuse Methods

Testing the same cell under varying conditions can also be used to establish the effect the abuse method, atmosphere, or SoC has on the gas composition. When subjected to multiple abuse methods under a N_2 atmosphere, H_2, CO_2, and CO were found to be the most abundant gases across external heat, overcharge, and nail penetration tests on 60 Ah pouch and prismatic cells [13]. CH_4, C_2H_4, C_2H_6, C_3H_6, and C_3H_8 were also detected. Similar results were also seen in tests by Xu, where the failure of 156 Ah prismatic and 52 Ah pouch cells using the same abuse methods resulted in H_2, CO, and CO_2 being the most abundant gases, the concentrations of which were quantified [21]. The prismatic cell produced the following: CO (25–35 vol%), CO_2 (18–32 vol%), and H_2 (25–35 vol%). The pouch cell produced CO (22–24 vol%), CO_2 (29–39 vol%), and H_2 (20–30 vol%). All alkenes and alkanes up to five carbon atoms long were also detected in the failure gas of the prismatic cell. The SoC can also impact gas composition, as Willstrand found that the concentrations of CO_2 and CO rose with the SoC when tested under inert conditions [14].

Although the effect of different abuse conditions, O_2 availability, and SoCs has been established, no study has produced a comprehensive dataset which focuses on one cell nor

reported the impact different test configurations have on the gas volume and composition produced during failure.

We present results produced from tests using all three abuse methods (external heat, overcharge, and nail penetration) in both air and N_2 atmospheres, as well as at a range of SoCs. We also report both gas volume and composition, with each test configuration performed in triplicate where practical. We also include the failure data of cell blocks containing an increasing number of cells failed using external heating in both air and N_2 atmospheres. This allows a direct comparison of the effect that the SoC, abuse method, and atmosphere have on gas composition and volume for one cell type.

2. Materials and Methods

2.1. Cell Characterisation

All tests were performed on a 5 Ah NMC pouch cell, which was cycled two times to 100% SoC prior to testing. For cells tested at an SoC other than 100%, an additional step was included to reach the desired SoC, and calculations were carried out via Coulomb counting. All cells were charged used an MTI charger (BST 8 5A CST). A sample of cells was taken to measure the internal resistance (IR) after the cell had been cycled and was at 100% SoC. IR measurements were taken using alternating current internal resistance (ACIR) at 1 kHz (Applent AT526). A summary of the cell characterisation details is shown in Table 1.

Table 1. Cell characterisation and cell charging routine.

Cell Characterisation		Charging Routine Parameters	
Nominal capacity (Ah)	5	Lower discharge voltage (V)	2.75
Nominal cell voltage (V)	3.65	Upper charge voltage (V)	4.2
Actual capacity (Ah)	4.8 *	Cut-off current (A)	0.5
Cell chemistry	NMC	Charge rate (CCCV) (A)	1.0
Internal resistance (mΩ)	32 *	Discharge rate (CC) (A)	1.0
Dimensions (mm)	60 × 90 × 5		
Weight (g)	76		

* Results given as an average of three tests.

Cathode Chemistry

The exact cathode chemistry of the cell was also determined prior to abuse testing. The cell was discharged to 0% SoC and disassembled, and a small section of the cathode was removed. Inductively coupled plasma atomic emission spectroscopy (ICP-AES) was used for bulk electrode analysis, X-ray fluorescence (XRF), and scanning electron microscopy with energy-dispersive X-ray spectroscopy (SEM-EDS) for surface electrode analysis.

ICP-AES analysis was performed by digesting the cathode using 3 mL HNO_3/2 mL HCl/0.25 mL HF at 95 °C for 1 h in a graphite heating block [22] Following the dilution of the digested material, subsequent analysis was performed by ICP-AES [23]. XRF analysis of the anode and cathode was also performed using a Thermo Scientific Niton Xl3t 700 analyser. The results showed no presence of silicon in the anode. The results of the ICP-AES and XRF analysis for the cathode are summarised in Table 2.

Table 2. ICP-AES and XRF elemental analysis results.

Element	ICP-AES (%wt.)	XRF (%wt.)
Ni	45.7	48.0
Co	11.7	11.6
Mn	42.6	39.7
Other	-	0.7

SEM-EDS analysis was performed using a Hitachi SU3500 SEM equipped with EDS operating at 20 kV. EDS elemental mapping was used to determine the distribution of elements. Four individual sections of the cathode were used for the EDS analysis, and the results given as an average percentage of the elements detected at each point. Figure 1 shows two types of differing compositions: Some grains appeared to be mixtures of all three cathode metals, with others being predominantly manganese only. Hence, it is presumed that this cathode is a blend of NMC and LMO (lithium manganese oxide). The approximate ratio of the NMC component was derived from an examination of the spectrum 4 region in Figure 1 and found to be approximately nickel–manganese–cobalt at 54:34:13. Combining the results of both ICP-AES and EDS suggests that the cathode is NMC with approximately 13% LMO.

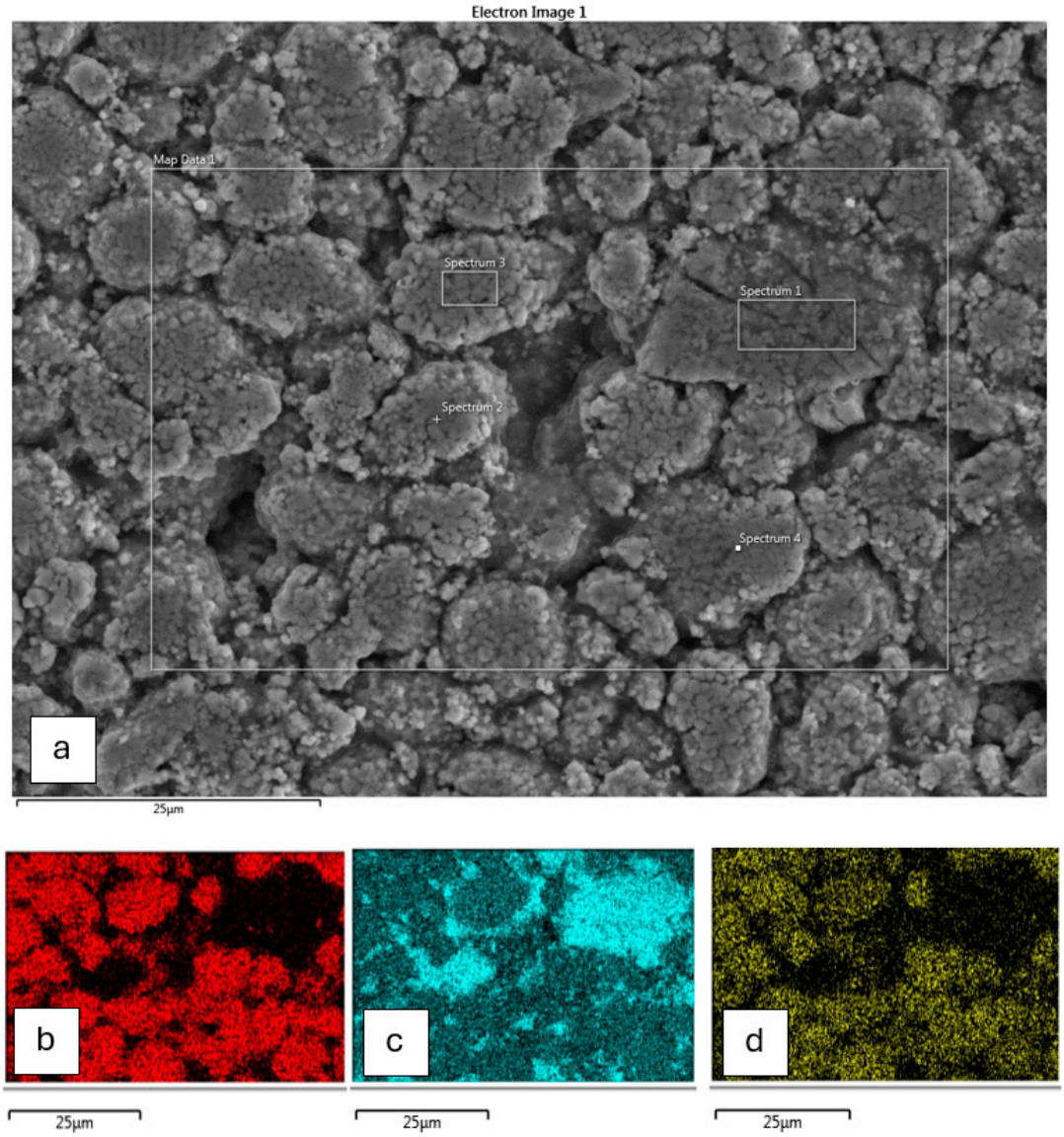

Figure 1. (**a**) Full EDS map of electrode foil showing the four key areas of analysis; (**b**) EDS mapping showing distribution of nickel; (**c**) EDS mapping showing distribution of manganese; (**d**) EDS mapping showing distribution of cobalt.

2.2. Test Method

To understand the effect different conditions had on gas volume production and composition, single cells were subjected to different abuse methods (external heat, overcharge, and nail penetration). Additional external heat tests were performed on cell blocks containing up to four cells.

All tests were conducted inside a 47 L pressure vessel rated to 10 bar at 200 °Choused within a blast cell and operated remotely. Type-N thermocouples (accuracy ± 2.2 °C) that were placed on the cell's surface, inside the pressure vessel (ambient temperature), above the cell, and on the outer surface of the pressure vessel were used to record the temperature throughout each test. To account for any potential temperature variation due to the accuracy of thermocouple measurements, the gas volume was recalculated for Test 3 and was calculated based on an error of ±2.2 °C. Based on these calculations, the error in gas volume was ±0.02 L. To prevent flame impingement on the inner surface of the pressure vessel, the cells were placed inside a baffle box during each test. Pressure measurements were taken using a 0–2 bar pressure transducer placed in the centre back of the vessel.

Both temperature and pressure measurements were recorded at a rate of 10 ms. Testing was performed in either an air or N_2 atmosphere, the latter of which was achieved by purging the vessel with N_2 seven times prior to testing. The N_2 used to purge the vessel (BOC Nitrogen (Oxygen-free), purity 99.998%) was taken from the same cylinder pack for all tests, minimising variations in the results. This created a N_2 atmosphere with a concentration of approximately 99.5%. The pressure vessel also passed a leak test before each test began. In total, 48 individual tests were performed under a range of different conditions, such as the abuse method, SoC, charge rate, and atmosphere. The details for these tests can be found below.

2.2.1. External Heat

Single cells at a 100% SoC were heated using a 3 × 2″ adhesive electrical heater (KHLVA-203/10-P, Omega, Manchester, UK) supplied with 60 W electrical power. The cell was constrained between a 6 mm calcium silicate fireboard and 6 mm stainless steel sheets bolted together in all four corners. Six tests in total were conducted, three in N_2 and three in air, with gas samples collected for two tests in each atmosphere. Two additional tests were performed at each of the following SoCs: 5%, 25%, 50%, and 75%. These were conducted in a N_2 atmosphere only, with gas samples collected for all tests.

Cell blocks made up of two, three, or four cells at 100% SoC were tested under a N_2 atmosphere, with only gas volume calculations performed. The initiator cell was heated in the same manner as the single cell tests, with the other cells in the block failing via propagation. A thermocouple was placed on the surface of the initiating cell opposite the heater. Throughout the tests, the cell blocks were constrained in the same way as the single cell tests.

2.2.2. Overcharge

Single cells at a starting SoC of 100% were overcharged under different test conditions, including different atmospheres, charging rates, and whether the cell was unconstrained or constrained (see external heat setup) to prevent swelling, to understand how these conditions affected gas volume and composition. The setup for each overcharge test and the number of repeats are summarised in Table 3.

Table 3. Summary of overcharge test setups.

Overcharge Rate (A)	Cell Constrained?	Atmosphere	Number of Tests	Number of Tests with Gas Samples
5 (1 C)	Yes	Air	3	2
5 (1 C)	Yes	N_2	3	2
5 (1 C)	No	Air	3	0
5 (1 C)	No	N_2	3	1
2.5 (0.5 C)	Yes	N_2	2	2
10 (2 C)	Yes	N_2	2	2

2.2.3. Nail Penetration

A custom test rig with an actuator was used to pierce the centre of the cell held vertically opposite the nail. The nail has a diameter of 4 mm with a point angle of 40°, travelling at a speed of approximately 1 cm/s. Six tests were conducted on the cell with a 100% SoC, three in N_2 and three in air. Two gas samples were collected for each atmosphere. Four additional tests were conducted in a N_2 atmosphere, two at 50% and two at a 75% SoC.

2.3. Gas Volume Calculation

The gas volume generated during cell failure was calculated from the pressure increase at cell failure using the ideal gas law. The ambient temperature and pressure recorded during the test were used to calculate the final gas volume. The initial moles of gas were calculated and normalized, accounting for the additional gas produced as a result of cell failure. The number of moles was then used to calculate the final gas volume. All gas volumes were normalized in order to be used relative to the standard atmospheric temperature and pressure (SATP) (298 K, 101,325 Pa), allowing for easier comparisons between tests.

2.4. Gas Composition Analysis

For tests where gas samples were collected, the pressure vessel was allowed to return to ambient temperature, and a fan was used to mix the gas, which remained on until the test was completed. Samples were then taken via a sampling vent and collected in a 5 L Tedlar gas bag. These were analysed within 24 h of sampling to reduce the leakage of the gas. Gas analyses were performed using a Hiden Analytical™ HRP-20 quadrupole mass spectrometer with a heated capillary tube. Raw data were converted into % volume by subtracting the contribution of overlapping fragment ions and converting them using the instrument's relative sensitivity factors for the target gas. Background subtraction was applied to the data prior to conversion. Data were collected over a 0–200 mass range and quantified: H_2, CO_2, CO, CH_4, C_2H_4, C_3H_6, and C_3H_8. If any other gases were present in the samples, it was assumed to be at very low concentrations and therefore negligible [12]. The analyser was controlled using MASsoft 10. Further details for the gas composition analysis calculations have previously been reported [23].

The equipment used and the test configuration for each test type are shown in Figure 2.

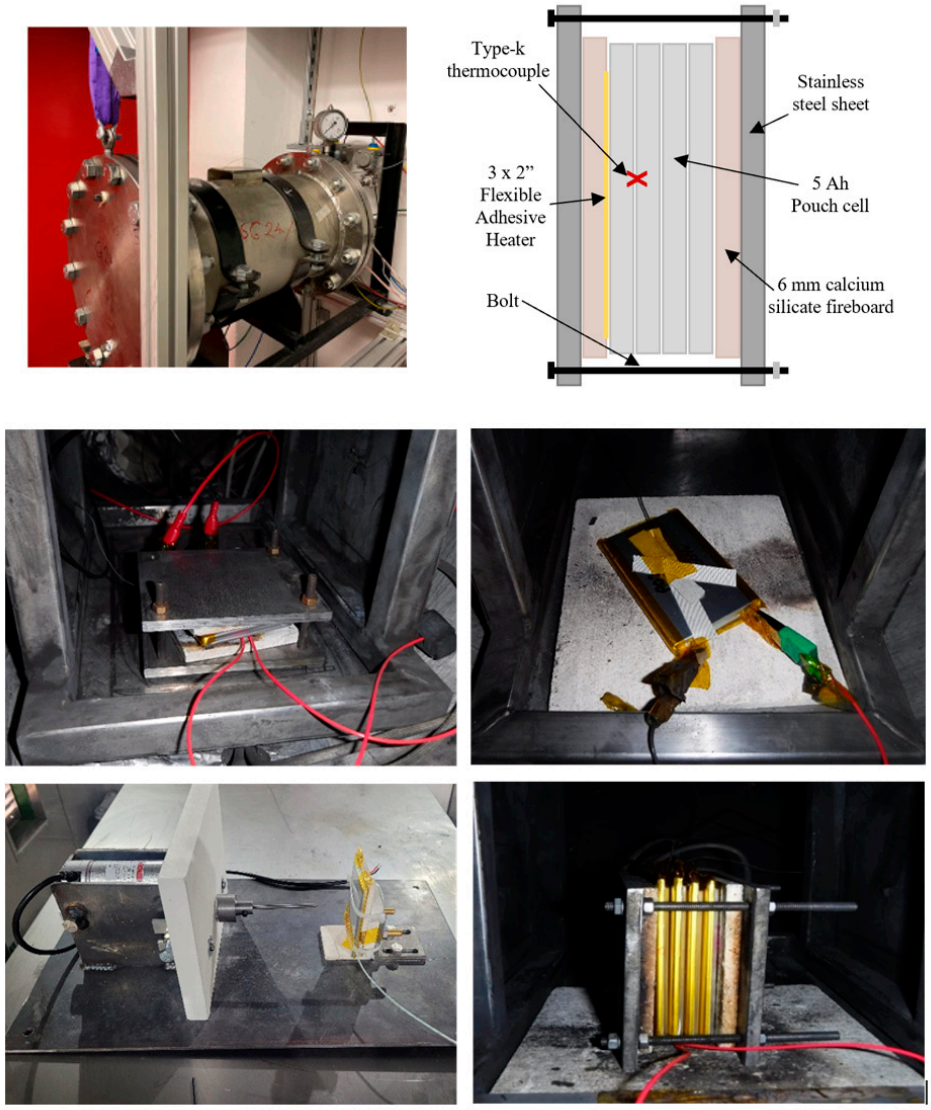

Figure 2. Pressure vessel used for all tests (**top left**), schematic of cell the block test (**top right**), constrained external heat test setup (**centre left**), unconstrained overcharge test setup (**centre right**), nail penetration test setup (**bottom left**), and external heat testof the four-cell block (**bottom right**).

3. Results and Discussion

Conducting tests with the same setup in air and N_2 atmospheres helps establish the difference in gas composition where combustion was possible (air atmosphere) or unlikely (N_2 atmosphere). The level of combustion is dependent on the O_2 concentration available, therefore affecting the composition of gas generated by the cells [24]. All gas volumes referenced have been calculated at SATP.

3.1. External Heat Gas Volume and Composition

3.1.1. SoC at 100%

The external heat tests were performed in triplicate for both atmospheres. For tests at a 100% SoC, the average gas volume generated in a N_2 atmosphere was 6.9 L (1.38 L/Ah), higher than the same tests in air, which generated 3.9 L (0.78 L/Ah) of gas (Table 4).

Table 4. Average net gas volume increase, average volume/Ah stored, and gas composition given as an average percentage for a single cell at 100% SoC relative to external heat tests in air and N_2 atmospheres.

Atmosphere	Average Net Gas Volume Increase (L)	Average Volume/Ah Stored (L/Ah)	Average v/v% Gas Composition							
			H_2	CO_2	CO	C_2H_6	C_2H_4	C_3H_8	C_3H_6	CH_4
Air	3.9	0.78	6.1	40.9	47.1	0.3	2.2	0.7	0.3	2.4
N_2	6.9	1.37	24.9	19.9	34.3	3.3	8.4	2.5	1.4	5.6

This difference is due to the availability of O_2 and its effect on combustion. During failure under an air atmosphere (21% O_2 concentration), the self-ignition and combustion of the gases generated occurred, resulting in the formation of CO_2 and H_2O vapour, the latter of which condenses when the vessel returns to ambient temperature, removing its contribution to the final gas volume and consuming a volume of O_2. Under a N_2 atmosphere, there is no O_2 for the combustion of flammable gases or the production of water vapour nor O_2 consumption. Any O_2 which may be produced during the failure of the cell is also likely to undergo combustion during failure regardless of the atmosphere, making its overall effect on gas volume and composition negligible [21].

Previous work on a 5 Ah NMC 21700 cell indicated that for complete combustion to occur, 7 L of O_2 was required. This figure was calculated based on the Ar:O_2 ratio from samples taken from inside the pressure vessel with an air atmosphere before a test and after cell failure [25]. O_2 detected by the failure of 12 and 18 cell blocks consisting of 2.6 Ah 18650 cells suggested that between 0.023 g and 0.028 g of O_2 was released per cell, equating to 0.0161 L and 0.0196 L (SATP), which is much less than the O_2 required to support combustion. Any O_2 that was detected was determined to be down to the degradation of the cathode material [26].

These effects can be seen when looking at the gas analysis results, where H_2 makes up a large proportion of the composition, 24.9%, in N_2 compared to 6.1% in air. The higher concentration of O_2 in the air atmosphere also allows for the generation of higher percentage volumes of CO_2 at 40.9% due to complete combustion, compared with 19.9% in a N_2 atmosphere. It is unusual that there is a higher 47.1% concentration of CO generated in an air atmosphere compared to 34.3% in a N_2 atmosphere. This is the opposite of the trend observed for comparable overcharge and nail penetration tests. The higher CO may be a result of the incomplete combustion of hydrocarbons, where insufficient O_2 supplies at the point of burning are a limiting factor. Despite insufficient O_2 for combustion in N_2, CO_2 and CO are still detected, which are most likely produced as a result of the chemical decomposition of organic electrolyte within the cell rather than the combustion process [21]. There were also higher percentage volumes of small hydrocarbons, CH_4, C_2H_4, C_2H_6, C_3H_6, and C_3H_8, as in a N_2 atmosphere, they are unable to combust.

A summary can be found in Table 4. The full results of all external heat tests can be found in the Supplementary Materials.

3.1.2. SoC at 75%, 50%, 25%, and 5%

The volume of gas generated by the failure of cells using external heating decreases with the SoC. In general, the average volume of gas generated per ampere hour remained consistent across SoCs, producing between 1.38 and 2.0 L. At the lowest SoC, 5%, some gas was still produced at a much greater volume per ampere: 8.0 L (Figure 3).

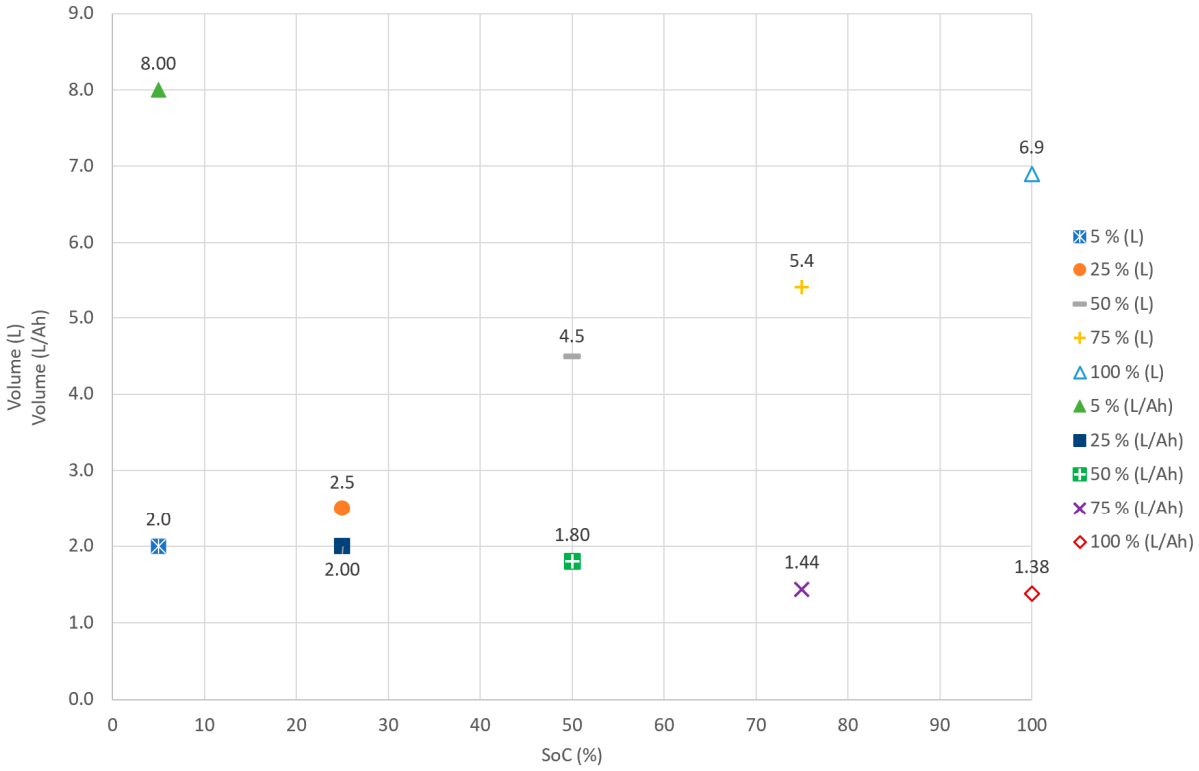

Figure 3. Average gas volume for external heat tests in a N_2 atmosphere for cells at a 5%, 25%, 50%, 75%, and 100% SoC.

The gas composition for the external heat tests at all SoCs in a N_2 atmosphere is shown in Table 5.

Table 5. Average net gas volume increase, average volume/Ah stored, and gas composition given as a percentage volume for external heat tests for cells at a 5%, 25%, 50%, and 75% SoC in a N_2 atmosphere.

SoC (%)	Average v/v% Gas Composition							
	H_2	CO_2	CO	C_2H_6	C_2H_4	C_3H_8	C_3H_6	CH_4
5	7.5	66.4	4.0	2.6	5.2	7.6	1.7	5.3
25	14.9	61.1	2.1	1.5	5.5	9.1	2.5	3.5
50	30.7	42.7	10.0	1.0	3.9	5.4	2.2	4.3
75	25.2	47.7	8.1	2.6	5.1	4.7	2.7	4.1
100	24.9	19.9	34.3	3.3	8.4	2.5	1.4	5.6

Gas composition analyses indicated that the relative percentage of H_2 produced during cell failure was generally consistently above 50% SoC, producing between 24.9 and 30.7% H_2; however, it did decrease at lower SoCs, producing a much smaller %volume, 7.5% at a 5% SoC. In general, the relative proportion of CO_2 increases with the SoC, in contrast to CO, which is significantly lower at all SoCs other than 100%, where it reached an average of 34.3%. The relative percentage of the small hydrocarbons identifed also remained consistent across all SoCs. Similarly, the increase in CO_2 concentration with increasing SoCs and similar hydrocarbon concentrations across all SoCs was observed by Willstrand; however, the opposite effect on CO and CO_2 concentration occurred, which may be due to differences in electrolyte compositions [14].

3.2. Cell Block Tests

3.2.1. Temperature Measurement

The initiating cell temperature was measured throughout the test, using a thermocouple attached to the cell's surface. The failure temperature of the initiating cell was not affected by the number of cells in the block or the pressure vessel's atmosphere, and it was found to be between 157 and 182 °C. Once failure of the initiator cell had occurred, a high enough temperature was sustained to send the remaining cells into thermal failure via propagation. The maximum temperature reached during the failure of the cell blocks was also consistent between all tests, reaching between 1010 and 1038 °C.

3.2.2. Pressure Measurement

Each pressure pulse in the data corresponds to failure on each cell, confirming their failure (Figure 4). In the air atmosphere, the initial peak, representing the failure of the first initiator cell, reached a higher sequential pressure compared to the subsequent cell failures. The combustion of flammable gases produced by the cells increases the sudden initial pressure peak due to the heat produced by the combustion of gas. After the initial failure, the O_2 concentration decreased to a level that prevented the combustion of gas produced by the remaining cells. The peaks observed are much smaller, as the peaks are due to gas production only. Overall, for the cells that failed under the air atmosphere, they likely underwent combustion-based propagation, with the ignition of the initial cell generating enough flames to start the combustion of other cells. In contrast, in the N_2 atmosphere, the pressure of each peak increased with each cell failure, as the cells are undergoing TR-based propagation, where the failure of the first cell was unlikely to result in flames. Therefore, the first cell acts as a heat source for the other cells, allowing them to undergo TR. No combustion event occurred at any point during the failure of these cell blocks due to insufficient O_2. Each pressure peak is at a higher pressure due to the increasing total gas volume from additional cell failures. The slight decrease between peaks is due to gas cooling and condensing between cell failures. This pattern in pressure peaks matches the results observed in the experiments conducted by Archibald on similar pouch cell block tests in an inert atmosphere only [27]. An example of the temperature and pressure profiles of the four cell blocks in N_2 and in air is shown in Figure 4.

3.2.3. Gas Volume

As before, all tests in N_2 have a higher gas volume than comparable air tests. This is due to the same failure mechanism occurring as described for a single-cell external heat test. These results are summarised in Figure 5.

3.3. Overcharge Test Results

3.3.1. State of Charge at Failure

Cells at 100% SoC were charged at a rate of 2.5, 5, or 10 A, with no maximum voltage limit, until cell failure. The failure SoC was approximated using Coulomb counting. The time a certain current was supplied to the cell was recorded, and this was multiplied by the time during which a number of amperes were delivered to the cell. This was then added to the starting capacity of 5 Ah, which allowed the capacity at cell failure to be calculated.

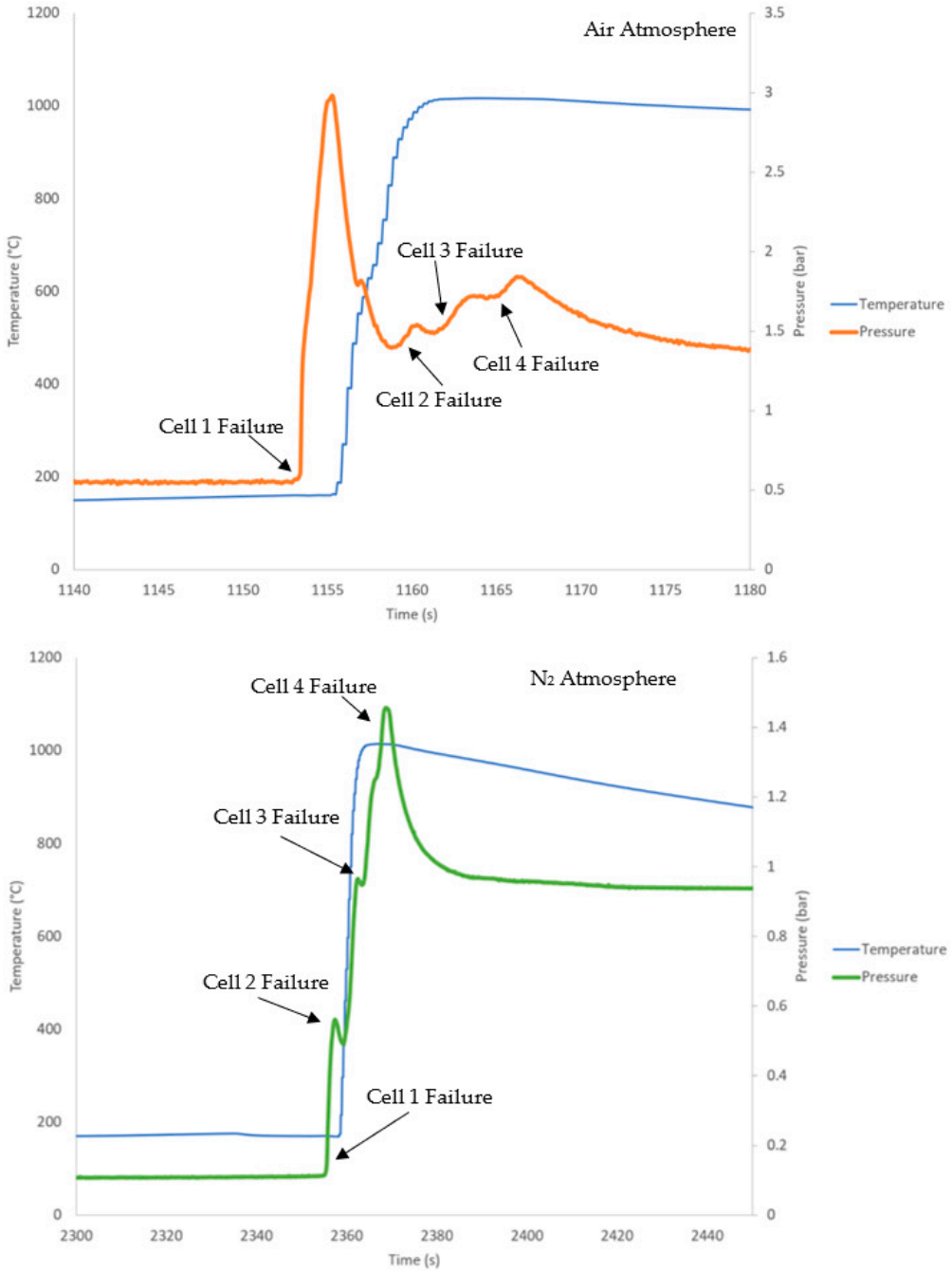

Figure 4. Temperature of the initiator cell (Cell 1) and pressure for a four-cell-block external heat test in an air atmosphere (top, orange) and a four-cell-block external heat test in a N_2 atmosphere (bottom, green).

In general, constrained and unconstrained cells that were charged at a rate of 5 A failed at a similar SoC and capacity: between 142% (7.46 Ah) and 150% (7.48 Ah). Only one of the 5 A tests (test 28) had a lower failure SoC at 122%. Cells at a higher charging rate of 10 A had a higher failure SoC of 187% and 192%, and those at 2.5 A were even lower, failing at 137%.

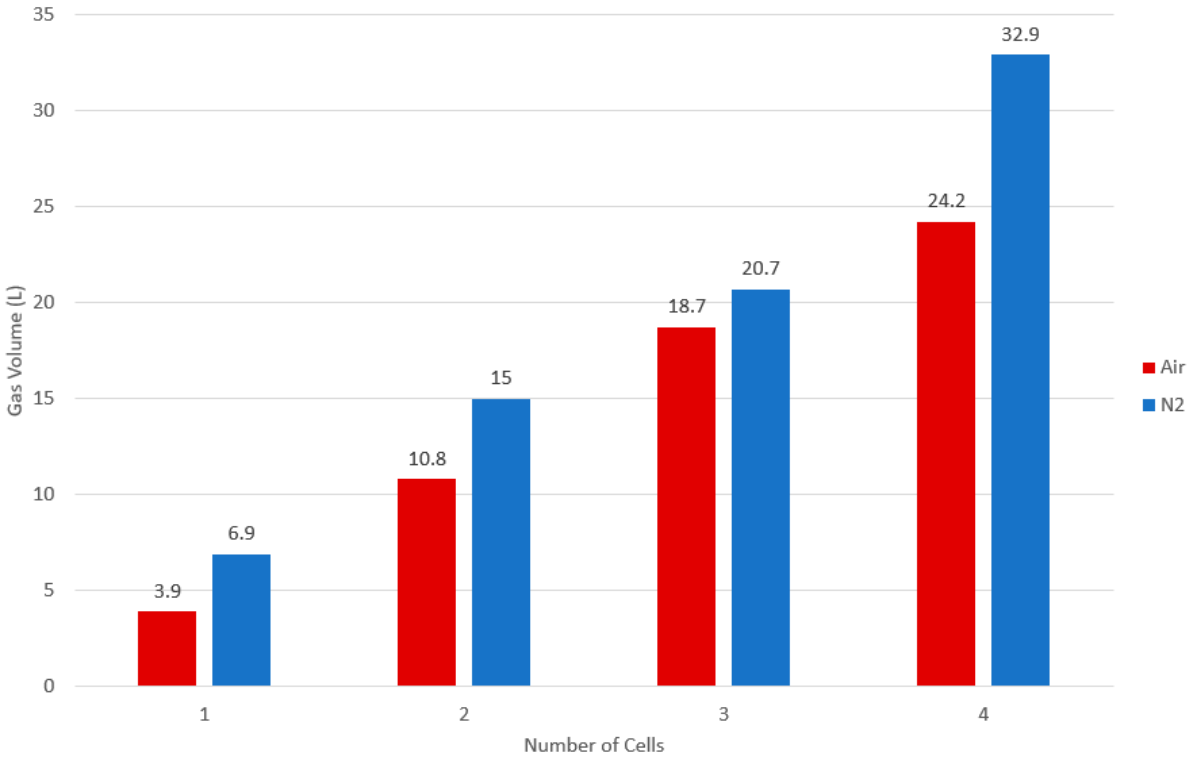

Figure 5. Gas volumes for the cell block tests. The results of the N_2 tests (red) are an average of 2 tests. The results of the air tests (blue) are from a single test.

3.3.2. Gas Volume and Composition

The average net gas volume and percentage volume gas composition for all overcharge test types are summarised in Table 6.

Table 6. Summary of individual overcharge tests gas volume, failure SoC, failure capacity, and volume/Ah stored. Note: Overcharge test 22 did not have SoC data as the cell voltage and power supply current were not recorded during the test.

Test Number	Charging Rate/Test Setupp	Gas Volume Increase (L)	Failure SoC (%)	Charge Stored at Failure (Ah)	Volume/Ah Stored at Failure (L)
15	5 A air constrained	7.0	149	7.46	0.94
16		5.9	148	7.40	0.80
17		6.3	143	7.15	0.88
18	5 A N_2 constrained	11.1	148	7.40	1.50
19		11.6	147	7.32	1.58
20		11.1	150	7.48	1.48
21	2.5 A N_2 constrained	11.5	137	6.83	1.68
22		12.3	-	-	-
23	10 A N_2 constrained	10.7	187	9.35	1.14
24		11.9	192	9.60	1.24
25	5 A air unconstrained	4.5	149	7.45	0.60
26		4.6	143	7.15	0.64
27		4.3	142	7.10	0.61
28	5 A N_2 unconstrained	11.6	122	6.10	1.90
29		11.3	143	7.15	1.58
30		11.9	142	7.10	1.68

Similarly to the external heat tests, both the 5 A constrained and 5 A unconstrained tests in air generated a smaller average gas volume, 6.4 L and 4.5 L, compared to the same test setup under a N2 atmosphere, which generated average gas volumes of 11.3 L and 11.6 L. Understanding the difference between the gas volumes generated when the cell is constrained compared to when it is not is important, as when they are used for real-life applications, they are often constrained within equipment. A study by Forestier found that constraining the cell impacted gas volumes and compositions during failure when heated to failure under an air atmosphere, with constrained cells generating a smaller volume of gas [28]. This contrasts with the results of this study, as the 5 A constrained tests in the air generated a higher gas volume compared to the unconstrained tests. This, however, was not observed for the tests in a N_2 atmosphere, where there was a minor difference in gas volume. For tests with different charging rates, there seemed to be a minor impact on the volume of gas generated (Table 7).

Table 7. Average net gas volume increase and gas analysis results for constrained and unconstrained tests at 5 A charging rates in air and N_2 and constrained tests at 2.5 A and 10 A rates in N_2. Note: The values of the 5 A rate unconstrained cell in N_2 are not averages due to only one test being conducted. Gas analysis data were also not collected for unconstrained cells charged at a 5 A rate under an air atmosphere.

Atmosphere Test Setup	Average Net Gas Volume Increase (L)	Average v/v% Gas Composition							
		H_2	CO_2	CO	C_2H_6	C_2H_4	C_3H_8	C_3H_6	CH_4
5 A Air **c**onstrained	6.4	8.3	38.5	46.2	1.3	2.5	0.5	0.4	2.6
5 A N_2 **c**onstrained	11.3	25.0	19.2	33.8	3.7	9.7	2.6	1.4	4.8
2.5 A N_2 **c**onstrained	11.9	26.9	35.0	16.4	3.3	10.4	3.2	1.6	3.5
10 A N_2 **c**onstrained	11.3	23.8	31.3	14.7	4.6	15.3	3.5	2.6	4.6
5 A N_2 **u**nconstrained	11.6	25.6	18.4	28.8	4.1	13.7	1.4	1.3	6.8

Gas composition data show a difference in gas percentage volume between air and N_2 atmospheres for constrained cells charged to failure at a 5 A rate. There was a higher percentage volume of H_2 for tests conducted in air, 8.3%, compared to those in N_2, 25%. This is likely due to the similar reaction mechanisms observed in the external heat tests.

The rate of charging for tests in a N_2 atmosphere also affects the gas composition. Tests conducted at a charging rate of 5 A produced less CO_2, 19.2%, than those at 2.5 A and 10 A, which produced 35% and 31.3%, respectively. Where more CO_2 was produced, there was a reduction in the CO percentage volume. The levels of H_2 and other small hydrocarbons remained broadly consistent between charging rates.

A final factor with the potential to affect gas compositions is whether the cell was constrained or not throughout the test. Comparisons between constrained and unconstrained cells charged at a rate of 5 A until failure in a N_2 atmosphere showed little effect on the percentage volume of all the gases identified. It should be noted that the figures for the unconstrained cell test were based on a single test, whereas those for constrained cells were taken as an average of the three tests conducted. Repeated testing on constrained cells was deemed to be more beneficial, as this is how they are likely to be found when used in "real-life" applications.

3.4. Nail Penetration Test Gas Volume and Composition

3.4.1. SoC at 100%

Cells at a 100% SoC were failed using nail penetration in both air and N_2 atmospheres. Tests were repeated in triplicate for each atmosphere, with gas volumes calculated for each test and gas samples collected after failure for two of the three tests. Mao has suggested that the maximum temperature reached by cells during failure has the potential to increase with the speed at which the nail was travelling [29]. This increase in temperature may have the potential to affect the final composition of the gas generated. We have provided data using tests performed with the same nail diameter, point angle, travelling at one speed, as the main focus was to compare the differences between failure mechanisms rather than differences in nail penetration test setups, e.g., nail diameter or speed. We have not investigated the potential effect of all variations on the total gas volume or composition.

A summary of the gas volume and composition is found in Table 8.

Table 8. Average net gas volume increase, average volume/Ah stored, and average relative percentage volume gas composition for nail penetration tests at a 100% SoC in both air and N_2 atmospheres.

Atmopshere	Average Net Gas Volume Increase (L)	Average Volume/Ah Stored (L)	Average v/v % Gas Composition							
			H_2	CO_2	CO	C_2H_6	C_2H_4	C_3H_8	C_3H_6	CH_4
Air	8.9	1.78	16.8	52.6	6.5	3.8	11.5	3.6	2.0	3.3
N_2	10.7	2.14	24.2	43.8	6.8	3.6	12.7	3.4	2.0	2.7

The average volume of gas generated under a N_2 atmosphere for nail penetration tests was 10.7 L, 1.8 L more than in an air atmosphere, which produced an average of 8.9 L. As before, the difference between atmospheres is likely to be a result of the O_2 concentrations affecting combustion rates, which was also seen in external heat and overcharge tests. When compared with other failure methods, the average gas volume for the nail penetration tests in air was higher; however, this is not true for tests in a N_2 atmosphere.

The gas composition for nail penetration tests in both air and N_2 atmospheres is similar, making it different compared to external heat and overcharge tests, where there are distinct composition differences between atmospheres. The key differences in the gas composition were the percentage volumes of H_2 and CO_2. A lower percentage volume of H_2 was generated in air at 16.8% compared to 24.2% in N_2, and the opposite was seen for CO_2, where the tests in N_2 produced a lower percentage volume at 48.2% compared with 52.6% in air. Despite these differences, there was little difference in gas concentrations for the remaining gases analysed between the atmospheres.

There were also notable differences in gas compositions for nail penetration and other failure mechanisms. There was a noticeably lower percentage volume of CO produced for both atmospheres in the nail penetration tests compared to similar overcharge tests and external heat tests at a 100% SoC. There was also a higher percentage volume of H_2 present in the nail penetration tests in the air atmosphere compared to similar external heat and overcharge tests. The final significant difference was in C_2H_4 production, with a higher percentage volume of C_2H_4 in both atmospheres compared to similar tests using different failure mechanisms. These differences in gas composition between failure mechanisms may be explained by the heat distribution throughout the test. For example, for external heat and overcharge tests, heat is distributed more evenly throughout the cell compared to nail penetration, where it can be more localised to the area where the nail has punctured the cell. There are also differences in the time taken to reach a cell's failure point between the different abuse mechanisms, with external heat and overcharge tests taking longer to reach cell failure and nail penetration tests having instantaneous failure. The difference in

time to reach failure may result in different reaction mechanisms and, therefore, different gas compositions.

3.4.2. SoC at 50% and 75%

During the two tests at 75% SoC and one at 50% SoC under a N_2 atmosphere, catastrophic failure was not observed, with no pressure increase observed in any test, indicating that no gas had been generated. There was a slight increase in temperature, with the maximum temperature of approximately 120 °C recorded from all three tests. Upon the removal of the 50% cell from the pressure vessel after the test, the nail had fully punctured the centre of the cell, and the cell had slightly swollen (Figure 6).

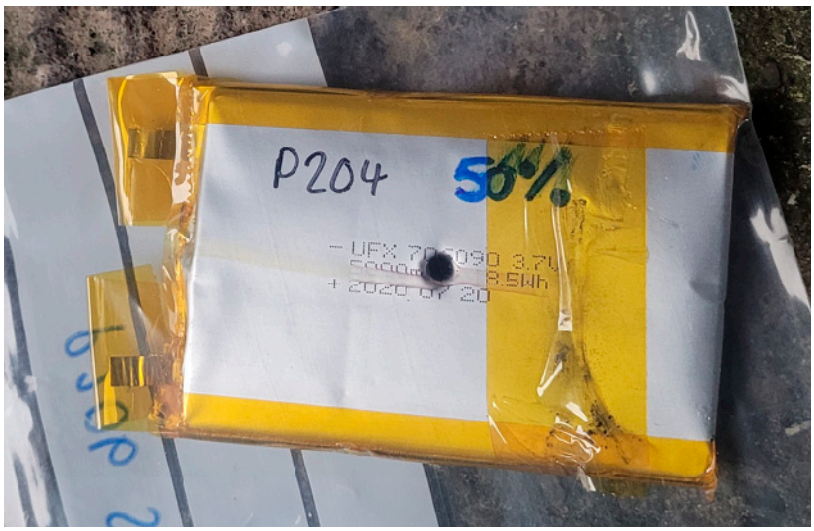

Figure 6. Swollen pouch cell after the nail penetration test at 50% SoC.

4. Conclusions

We have conducted a study comparing the different failure initiation mechanisms of a single cell type in both inert and air atmospheres, with the latter providing enough O_2 to support the complete combustion of a single cell. Furthermore, it included the investigation of multiple SoCs in one failure mode. A summary of all single-cell average gas volumes is shown in Figure 7.

All tests conducted in air produced a lower net average in gas volume than comparable tests in N_2 due to the combustion of flammable gases produced. Nail penetration and overcharge tests in N_2 produced similar volumes, which were approximately double the volume of external heat. In air, external heat tests produced the lowest amount of gas, and nail penetration produced the greatest amount. It is not currently clear why the differences between the abuse methods vary.

Overall, this demonstrates that the initiation method of cell failure may have a significant effect on the volume of gas generated. The composition of gas generated by cells at a 100% SoC does not seem to widely vary depending on the initiation method; however, the SoC has a larger effect, as shown by the results of the external heat tests at varying SoCs. The results found in this study show that several initiation methods should be evaluated for a better understanding of the gas produced from the failure of any cell type. Whilst the approximation of 2 L/Ah of total gas evolved would appear to hold true for the results we present and whilst generalised approximation can be useful, where it forms part of a safety evaluation, the failure of cells should be investigated by a variety of failure initiations.

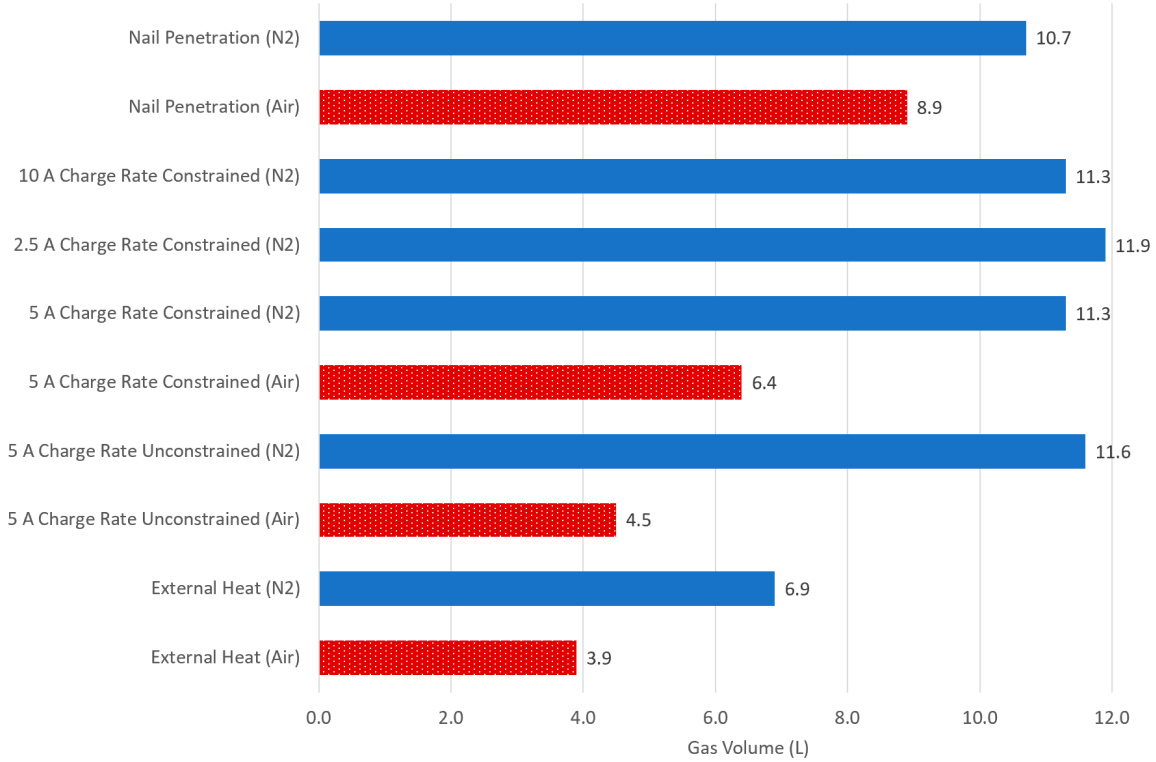

Figure 7. Summary of the average volume of gas generated for single cells at a 100% SoC in N_2 or air atmospheres.

Supplementary Materials: The following supporting information can be downloaded at https://www.mdpi.com/article/10.3390/batteries11050197/s1. Supplementary Data S1: Summary of all tests including temperature, gas volume, and gas composition data.

Author Contributions: G.E.H.: Writing—original draft, writing—review and editing, investigation, formal analysis, and validation. K.C.A.: Investigation. J.E.H.B.: Conceptualisation, funding acquisition, supervision, and writing—review and editing. J.G.: Investigation and conceptualisation. S.L.G.: Investigation. D.H.: Investigation. All authors have read and agreed to the published version of the manuscript.

Funding: The work is conducted within the framework of the "Lithium-Ion Battery Research In Safety (LIBRIS)" project funded by Innovate UK (Project No. 105296).

Data Availability Statement: The data presented in this study are available in the article and Supplementary Materials.

Acknowledgments: The authors would like to thank Darren Musgrove, from the HSE Science and Research Centre, for carrying out the ICP-AES analysis. The authors would like to thank Aneta Nemcova, from the HSE Science and Research Centre, for carrying out SEM-EDS and XRF analyses. The authors would like to thank Robert Richardson, from the HSE Science and Research Centre, for carrying out technical and editorial reviews.

Conflicts of Interest: The authors declare that they have no known competing financial interest or personal relationships that could have appeared to influence the work reported in this paper.

Abbreviations

LiB	Li-ion battery
EV	Electric vehicle
BESS	Battery energy storage system
SoC	State of charge
TR	Thermal runaway
NMC	Nickel manganese cobalt oxide
IR	Internal resistance
ACIR	Alternating current internal resistance
CCCV	Constant current constant voltage
CC	Constant current
ICP-AES	Inductively coupled plasma atomic emission spectroscopy
XRF	X-ray fluorescence
SEM-EDS	Scanning electron microscopy–energy-dispersive spectroscopy
LMO	Lithium manganese oxide
SATP	Standard atmosphere temperature and pressure

References

1. Sasse, T.; Rutter, J.; Shepheard, M.; Norris, E. *Net Zero: How Government Can Meet Its Climate Change Target*; Institute for Government: London, UK, 2020.
2. Gopinadh, S.V.; Anoopkumar, V.; Ansari, M.J.N.; Srivastava, D.; John, B.; Samridh, A.; Vijayakumar, P.S.; Mercy, T.D. Lithium-ion Pouch Cells: An Overview. In *Energy Harvesting and Storage*; Springer: Berlin/Heidelberg, Germany, 2022; pp. 209–224.
3. Feng, X.; Ouyang, M.; Liu, X.; Lu, L.; Xia, Y.; He, X. Thermal runaway mechanism of lithium ion battery for electric vehicles: A review. *Energy Storage Mater.* **2018**, *10*, 246–267. [CrossRef]
4. Yuan, L.; Dubaniewicz, T.; Zlochower, I.; Thomas, R.; Rayyan, N. Experimental study on thermal runaway and vented gases of lithium-ion cells. *Process Saf. Environ. Prot.* **2020**, *144*, 186–192. [CrossRef]
5. Kim, J.; Mallarapu, A.; Finegan, D.P.; Santhanagopalan, S. Modeling cell venting and gas-phase reactions in 18650 lithium ion batteries during thermal runaway. *J. Power Sources* **2021**, *489*, 229496. [CrossRef]
6. Mikolajczak, C.; Kahn, M.; White, K.; Long, R.T. Lithium-ion Battery Failures. In *Lithium-ion Batteries Hazard and Use Assessment*; Springer: Berlin/Heidelberg, Germany, 2012; pp. 43–70.
7. Howard, G.; Buston, J.; Gill, J. Experimental understanding of gas volumes and forces generated due to swelling during lithium-ion pouch cell failure. In Proceedings of the Hazards 31, Virtual, 16–18 November 2021.
8. Dubaniewicz, T.H.; Barone, T.L.; Brown, C.B.; Thomas, R.A. Comparison of thermal runaway pressures within sealed enclosures for nickel manganese cobalt and iron phosphate cathode lithium-ion cells. *J. Loss Prev. Process Ind.* **2022**, *76*, 104739. [CrossRef]
9. Koch, S.; Fill, A.; Birke, K.P. Comprehensive gas analysis on large scale automotive lithium-ion cells in thermal runaway. *J. Power Sources* **2018**, *398*, 106–112. [CrossRef]
10. Wei, N.; Li, M. Experimental study of thermal runaway process of 256Ah prismatic nickel-rich battery. *Front. Energy Res.* **2023**, *11*, 1230429. [CrossRef]
11. Yan, H.; Ezekoye, O.A. State of charge effects on active material elemental composition changes between pre-thermal-runaway and post-failure states for 8-1-1 nickel-manganese-cobalt 18650 cells. *J. Power Sources* **2023**, *63*, 106974. [CrossRef]
12. Sturk, D.; Rosell, L.; Blomqvist, P.; Tidblad, A.A. Analysis of Li-Ion Battery Gases Vented in an Inert Atmosphere Thermal Test Chamber. *Batteries* **2019**, *5*, 61. [CrossRef]
13. Essl, C.; Golubkov, A.W.; Fuchs, A. Comparing Different Thermal Runaway Triggers for Two Automotive Lithium-Ion Battery Cell Types. *J. Electrochem. Soc.* **2020**, *167*, 130542. [CrossRef]
14. Willstrand, O.; Pushp, M.; Andersson, P.; Brandell, D. Impact of different Li-ion cell test conditions on thermal runaway characteristics and gas release measurements. *J. Energy Storage* **2023**, *68*, 107785. [CrossRef]
15. Zou, K.; Lu, S.; Chen, X.; Gao, E.; Cao, Y.; Bi, Y. Thermal and gas characteristics of large-format $LiNi_{0.8}Co_{0.1}Mn_{0.1}O_2$ pouch power cell during thermal runaway. *J. Energy Storage* **2021**, *39*, 102609. [CrossRef]
16. Yuan, Q.; Zhao, F.; Wang, W.; Zhao, Y.; Liang, Z.; Yan, D. Overcharge failure investigation of lithium-ion batteries. *Electrochim. Acta* **2015**, *178*, 682–688. [CrossRef]
17. Cai, T.; Valecha, P.; Tran, V.; Engle, B.; Stefanopoulou, A.; Siegel, J. Detection of Li-ion battery failure and venting with Carbon Dioxide sensors. *eTransportation* **2021**, *7*, 100100. [CrossRef]

18. Koch, S.; Birke, K.P.; Kuhn, R. Fast Thermal Runaway Detection for Lithium-Ion Cells in Large Scale Traction Batteries. *Batteries* **2018**, *4*, 16. [CrossRef]
19. Nedjalkov, A.; Meyer, J.; Köhring, M.; Doering, A.; Angelmahr, M.; Dahle, S.; Sander, A.; Fischer, A.; Schade, W. Toxic Gas Emissions from Damaged Lithium Ion Batteries—Analysis and Safety Enhancement Solution. *Batteries* **2016**, *2*, 5. [CrossRef]
20. Hoelle, S.; Scharner, S.; Asanin, S.; Hinrichsen, O. Analysis on Thermal Runaway Behavior of Prismatic Lithium-Ion Batteries with Autoclave Calorimetry. *J. Electrochem. Soc.* **2021**, *168*, 120515. [CrossRef]
21. Xu, C.; Fan, Z.; Zhang, M.; Wang, P.; Wang, H.; Jin, C.; Peng, Y.; Jiang, F.; Feng, X.; Ouyang, M. A comparative study of the venting gas of lithium-ion batteries during thermal runaway triggered by various methods. *Cell Rep. Phys. Sci.* **2023**, *4*, 101705. [CrossRef]
22. *ISO15202-2:2012*; Workplace Air—Determination of Metals and Metalloids in Airborne Particulate Matter by Inductively Coupled Plasma Atomic Emission Spectrometry Part 2: Sample Preparation. ISO: Geneva, Switzerland, 2012.
23. *ISO 15202-3:2004*; Workplace Air—Determination of Metals and Metalloids in Airborne Particulate Matter by Inductively Coupled Plasma Atomic Emission Spectrometry Part 3: Analysis. ISO: Geneva, Switzerland, 2004.
24. Baird, A.R.; Archibald, E.J.; Marr, K.C.; Ezekoye, O.A. Explosion hazards from lithium-ion battery vent gas. *J. Power Sources* **2020**, *446*, 227257. [CrossRef]
25. Abbott, K.C.; Buston, J.E.; Gill, J.; Goddard, S.L.; Howard, D.; Howard, G.; Read, E.; Williams, R.C. Comprehensive gas analysis of a 21700 Li($Ni_{0.8}Co_{0.1}Mn_{0.1}O_2$) cell using mass spectrometry. *J. Power Sources* **2022**, *539*, 231585. [CrossRef]
26. Said, A.O.; Lee, C.; Stoliarov, S.I.; Marshal, A.W. Comprehensive analysis of dynamics and hazards associated with cascading failure in 18650 lithium ion cell arrays. *Appl. Energy* **2019**, *248*, 415–428. [CrossRef]
27. Archibald, E.; Kennedy, R.; Marr, K.; Jeevarajan, J.; Ezekoye, O. Characterization of Thermally Induced Runaway in Pouch Cells for Propagation. *Fire Technol.* **2020**, *56*, 2467–2490. [CrossRef]
28. Laruelle, S.; Forestier, C.; Lecocq, A.; Zantman, A.; Grugeon, S.; Sannier, L.; Marlair, G. Study of the Role of $LiNi_{1/3}Mn_{1/3}Co_{1/3}O_2$/Graphite Li-Ion Pouch Cells Confinement, Electrolyte Composition and Separator Coating on Thermal Runaway and Off-Gas Toxicit. *J. Electrochem. Soc.* **2020**, *167*, 090513. [CrossRef]
29. Mao, B.; Chen, H.; Cui, Z.; Wu, T.; Wang, Q. Failure mechanism of the lithium ion battery during nail penetration. *Int. J. Heat Mass Transf.* **2018**, *122*, 1103–1115. [CrossRef]